Facile route to implement transformation strengthening in titanium alloys

Guohua Zhao[a,*], Xin Xu[b,c,*], David Dye[b], Pedro E.J. Rivera-Díaz-del-Castillo[d], Nik Petrinic[a]

[a]*Department of Engineering Science, University of Oxford, Parks Road, Oxford OX1 3PJ, UK*
[b]*Department of Materials, Imperial College London, South Kensington, London SW7 2AZ, UK*
[c]*School of Materials, Sun Yat-Sen University, Shenzhen 518107, China*
[d]*Department of Engineering, Lancaster University, Lancaster LA1 4YW, UK*

Abstract

Developing lighter, stronger and more ductile aerospace metallic materials is in demand for energy efficiency strategies. Alloys with twinning-induced plasticity (TWIP) and/or transformation-induced plasticity (TRIP) effects have been exploited to defeat the conflict of strength versus ductility, yet very few if any physically informed methods exist to address the complex interactions between the transitions. Here we report a facile route to deploy transformation-mediated strengthening in Ti alloys, which particularly focuses on the supervised activation of TRIP and TWIP via a mechanism-driven modelling approach. New alloys were comparatively developed and presented notable resistances to strain localisation, but interestingly through distinct mechanical characteristics. Specifically, extraordinary strain-hardening rate ($d\sigma/d\varepsilon$) with a peak value of 2.4 GPa was achieved in Ti-10Mo-5Nb (wt.%), resulting from the synergetic activation of hierarchical transformations. An efficient model integrating TRIP and TWIP was applied to understand the interplays of the transition mechanisms.

Keywords: Ti alloys; Alloy design; TRIP/TWIP; Mechanism-driven modelling; Transformation strengthening

The quest of fuel-efficient and low-emission future propulsion systems motivates the discovery of new metallic materials with higher strength, lower density, superior toughness and durability [1]. Although conventional metals, e.g. aluminium alloys, are substantially replaced by carbon fibre reinforced composites, metals remain irreplaceable in safety-critical components with the highest requirements for reliability [2]. Aerospace engineering designs ask for the development of titanium alloys presenting excellent integrity of impact resilience, fracture toughness, fatigue resistance and stiffness while minimising weight. A route to simultaneously improve strength and ductility relies on the implementation of transformation-induced strengthening. Here the term *transformation* is used in a general sense to mean extensive rearrangement of the atomic structure. It is intended to include plastic deformation via deformation twinning because of the highly ordered nature of the rearrangement and the creation of coherent interface, which are closely relative

to martensitic transformation [3].

TRIP/TWIP Ti alloys with synergetic activation of $\beta \rightarrow \alpha''$ martensitic transformation and $\{332\}\langle113\rangle$ twinning display excellent deformation energy absorbing capacity in terms of superior strain-hardening and resistance to strain localisation [4, 5, 6]. The metastable bcc β phase may transform martensitically into orthorhombic α'' phase, while the strain-induced $\beta \rightarrow \alpha''$ transition presents easy reversibility after stress release [7, 8]. Such feature makes the direct measurement of the amount of $\beta \rightarrow \alpha''$ challenging, since the α'' martensite may hardly retain in the β matrix [9]. *In situ* neutron diffraction was applied to quantitatively determine the volume fraction changes of α'' phase ($f_{\alpha''}$) over strain in a representative TRIP/TWIP alloy Ti-12Mo (wt.%, same afterwards except further specifications)[10]. The result suggested $f_{\alpha''}$ reached 13.7 % at the early deformation stage then most of the α'' preserved in the microstructure after the stress release, yet it was difficult to tell whether the retained α'' existed inside the β matrix or within microstructural features such as twin bands. The followed transmission electron microscopy (TEM) observations showed the diffraction patterns of α'' and $\{332\}\langle113\rangle$ twin were overlapped to each other, which indicated the α'' closely coexisted with the twin. On the other hand, *In situ* synchrotron X-ray diffraction on superelastic Ti-27Nb (at.%) revealed that β completely transformed to α'' at the strain $\varepsilon = 0.03$ [11]. Interestingly, fully reversible $\alpha'' \rightarrow \beta$ transition took place after unloading, where β phase is restored with a large occurrence of $\{332\}\langle113\rangle$ twin. The studies suggested the transformability and the reversibility of $\beta \rightarrow \alpha''$ martensitic transformation are strongly composition-dependent. While it is widely appreciated that both $\beta \rightarrow \alpha''$ and twinning transitions play important roles in strain-hardening, however, very few if any physics-based models exist to address the complexity of transition interactions. Therefore it is crucial to establish an integrated method to reflect the role of each deformation mode to the overall mechanical properties.

In this work, we aim to design and deploy transformation strengthening in Ti alloys via a mechanism-driven modelling strategy. It enables the manipulation of TWIP and TRIP, and hence optimising the mechanical properties. We recently showed that the strain-hardening in TWIP Ti alloys stems from the emerging twin obstacles, where the reduced dislocation mean free path can be effectively controlled by the twinning kinetics [12]. In contrast, the joint TRIP/TWIP triggers hierarchical deformation and further promotes transformation strengthening. A model describing TRIP and TWIP was applied to unveil the deformation microstructure evolution, and quantitatively predicted the strengthening explicitly induced by martensitic transformation. Our route avoids expensive computations by using a set of physics-based parameters and simplified internal variables which are capable to reflect the β stability and deformation conditions.

Here we specifically proposed Ti-14Mo-5Sn and Ti-10Mo-5Nb alloys (wt.%) to exploit the composition-sensitive deformation mechanisms. The master alloys were prepared from pure elements by arc-melting in a low pressure, high-purity argon atmosphere. The ingots was hot shape-rolled above the β transus temperature and then solution-treated at 900 °C for 30 min followed by quenching. Uniaxial tensile tests were
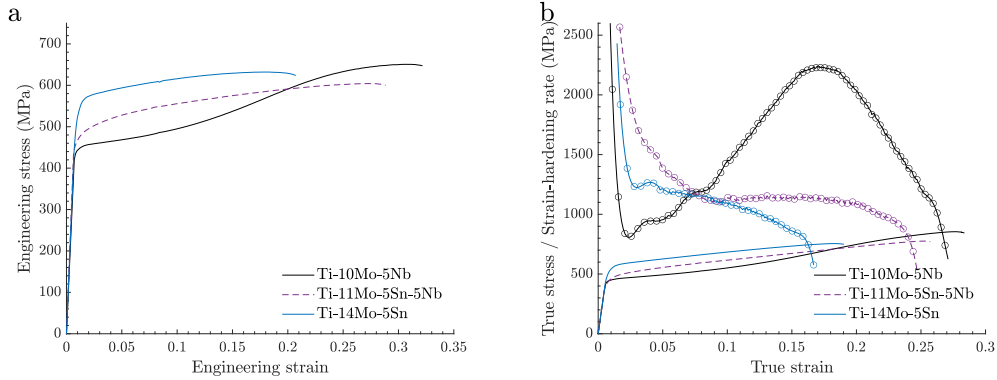
Figure 1: (a) Engineering stress-strain curve of Ti-14Mo-5Sn and Ti-10Mo-5Nb alloys under quasi-static strain rate $\dot{\varepsilon} = 5.0 \times 10^{-4}$ s^{-1}. The stress-strain curve of Ti-11Mo-5Sn-5Nb TWIP alloy [12] is displayed for comparison. (b) True stress-strain curves and the corresponding strain-hardening rate $\theta = d\sigma/d\varepsilon$ bullet plots.

performed with an extensometer along the rolling direction under a constant strain rate of $\dot{\varepsilon} = 5.0 \times 10^{-4}$ s^{-1}. Interrupted tests were conducted for Ti-14Mo-5Sn at the strain of 1.5%, 4.1% and 8.3%. The deformation microstructure was observed using a field-emission scanning electron microscope (ZEISS Sigma) equipped with an orientation imaging system for conducting the electron backscattered diffraction (EBSD) analysis. The data was acquired and post-processed using Bruker QUANTAX software. The step size was 0.2 μm and the total scanning map size was 286.4×214.8 μm^2. The pole figures were calculated using 100–140 pixels.

Fig.1 shows the tensile engineering stress-strain curves and the corresponding strain-hardening rate plots of Ti-14Mo-5Sn and Ti-10Mo-5Nb at quasi-static strain rate. The mechanical features of Ti-11Mo-5Sn-5Nb TWIP alloy from the previous work [12] is displayed for comparison. Ti-10Mo-5Nb exhibited a relatively lower yield stress but followed by superior plasticity via pronounced strain-hardening (Fig.1a). Uniform elongations (uEL) are adopted to describe the tensile plasticity and the values are approximated by the Considère criterion [13]. The uEL of Ti-10Mo-5Nb reached 0.27 ± 0.02 compared to 0.16 ± 0.01 of Ti-14Mo-5Sn (Fig.1b). It is worth noting the two alloys displayed distinct strain-hardening rate. Ti-14Mo-5Sn showed monotonically reduced $d\sigma/d\varepsilon$ over strain, which is allied to most of the TWIP alloys [12]. In contrast, Ti-10Mo-5Nb displayed a hump-shape $d\sigma/d\varepsilon$ feature which dynamically increased after yielding then reached a maximum of 2.4 GPa at $\varepsilon = 0.18$. Such characteristic is analogous to the reported TRIP/TWIP alloys [4, 14, 15, 7].

Fig.2 displays the EBSD microstructural evolution of Ti-14Mo-5Sn at different strains. The average grain size is 128 μm with a standard deviation of 56 μm. Thin $\{332\}\langle113\rangle$ twin bands appeared at the initial stage of plastic deformation (1.5% strain). The number of twins increased rapidly to accommodate the strain increase. Twin-twin intersections and twinning transfer through grain boundaries were observed at 8.3% strain. A characteristic feature of $\{332\}\langle113\rangle$ twin is that its width may grow broadly (for instance to over
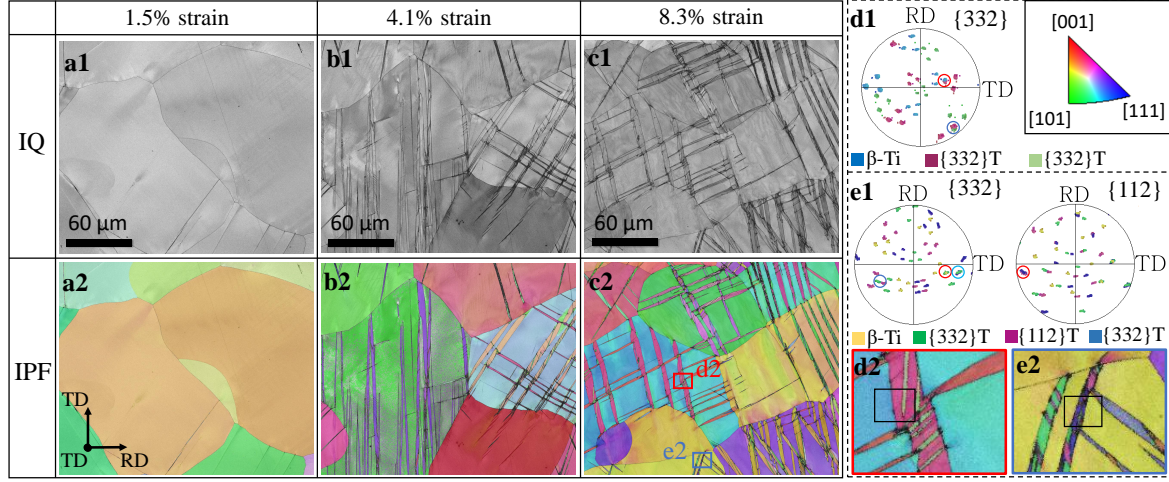
3

Figure 2: Deformation microstructures of Ti-14Mo-5Sn at different strain levels. EBSD image quality (IQ) maps and inverse pole figure (IPF) maps at engineering strains of (a1 and a2) 1.5%, (b1 and b2) 4.1% and (c1 and c2) 8.3%. (d1 and d2) Pole figure of $\{332\}\langle113\rangle$ twinning to the detected area. (e1 and e2) Pole figures of both $\{332\}\langle113\rangle$ and $\{112\}\langle111\rangle$ systems corresponding to the detected areas.

1.6 μm [16]), which is capable for the formation of hierarchical structures inside the primary twin. Pole figure analysis in Fig.2d and e exhibited the major substructures were secondary $\{332\}\langle113\rangle_{2nd}$ twins whereas very little $\{112\}\langle111\rangle_{2nd}$ system was identified adjacent to the $\{332\}\langle113\rangle_{2nd}$ ones. The $\{332\}\langle113\rangle_{2nd}$ formed preferably close to the twin-twin intersections, which accommodated local stress concentrations and may further enhance plasticity [17]. Fig.3 shows the deformation microstructure of Ti-10Mo-5Nb at the strain of fracture. The primary twinning bands were confirmed as $\{332\}\langle113\rangle$ system by the pole figure analysis in Fig.3c and e. The phase map in Fig.3b observed a noticeable amount of orthorhombic α'' martensite retained in some of the grains after stress release. The enlarged areas in Fig.3d1 and f1 further identified the α'' domains only appeared within the primary twinning bands, where most of the α'' coexisted with the neighbouring secondary $\{332\}\langle113\rangle_{2nd}$ twins. In contrary, α'' can hardly be observed in the matrix, which may fully reverse back to β phase [18] or retain small amounts in the microstructure [10].

It is essential to comparatively model the mechanical behaviours of TWIP and TRIP/TWIP Ti alloys, since the deformation modes are analogous but the two types of alloys present distinct strain-hardening rate. Given by the TWIP plasticity is attributed to the shear strain of twinning, the strain increment $d\varepsilon$ is facilitated by dislocation slip $d\varepsilon_{dis}$ and twinning strain by: $d\varepsilon = (1 - f_{tw})d\varepsilon_{dis} + \varepsilon_{tw}df_{tw}$, where f_{tw} is the volume fraction of $\{332\}\langle113\rangle$ twinning and ε_{tw} is the twinning strain. The promoted plasticity in TRIP/TWIP alloys is mediated by the collective operation of dislocation slip, twinning and martensitic transformation: $d\varepsilon = (1 - f_{tw} - f_{\alpha''})d\varepsilon_{dis} + \varepsilon_{tw}df_{tw} + f_{\alpha''}d\varepsilon_{\alpha''}$, where $d\varepsilon_{\alpha''}$ is the extra strain increment led by $\beta \rightarrow \alpha''$ transition. The strain-hardening during the plastic deformation is governed by the competition between dislocation
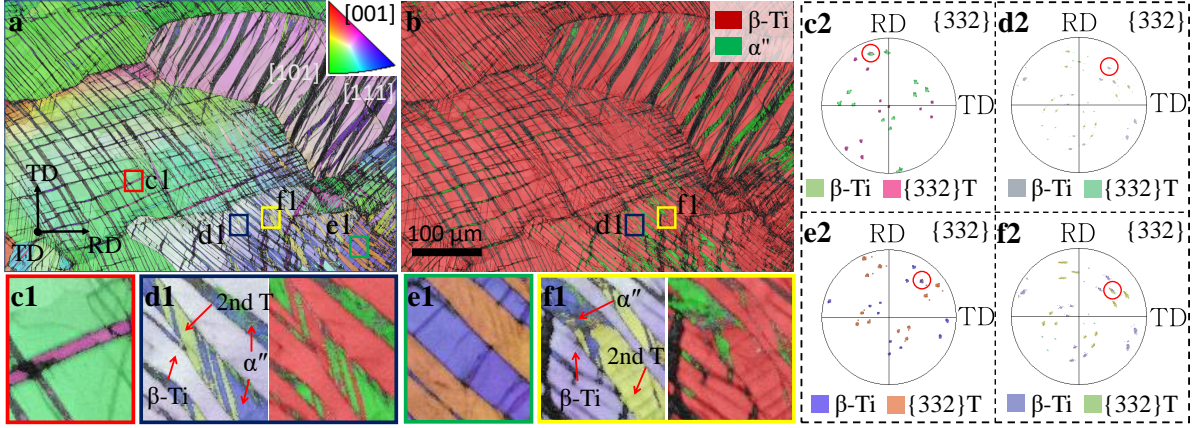
Figure 3: Deformation microstructure of Ti-10M-5Nb at the strain of fracture. (a) EBSD IPF map shows extensive deformation twinning. (b) The phase map reveals the retained α'' martensite after stress release. (c1 and c2) Detected twinning area and the corresponding pole figure present the primary $\{332\}\langle113\rangle$ twinning system. (d1 and d2) IPF, Phase map and the pole figure display the formation of hierarchical $\{332\}\langle113\rangle$ twin and α'' martensite. (e1 and e2) IPF and the pole figure confirm most of the primary products are $\{332\}\langle113\rangle$ twins. (f1 and f2) The retained α'' coexisted with neighbouring $\{332\}\langle113\rangle_{2nd}$ twin.

storage and annihilation, which can be described by the evolution rate of dislocation density $\frac{d\rho}{d\varepsilon}$. The dynamically created twin and martensite interfaces further reinforce the dislocation accumulation by reducing the dislocation mean free path. An integrated constitutive model has been derived incorporating transformation-enhanced isotropic hardening and kinematic hardening: $\sigma = \sigma_0 + \alpha M \mu b \sqrt{\rho} + M\mu b \left(\frac{1}{2t_{tw}} \frac{f_{tw}}{1-f_{tw}} + \frac{1}{D}\right)n$, where σ_0 comprises of the critical resolved shear stress of pure Ti, solid solution hardening and grain boundary strengthening [19], α reflects the average strength of dislocation interactions, b the Burgers vector, μ the shear modulus, D the grain size, n the number of dislocation loops on a given slip plane and t_{tw} the average width of deformation twinning. The detailed principles and methods for the formula derivation have been reported in the authors' work [20]. The strain-hardening rate can be solved analytically taking the dislocation density ρ as an internal variable:

$$\frac{d\sigma}{d\varepsilon} = \frac{d\sigma}{d\rho}\frac{d\rho}{d\varepsilon} = \frac{\alpha M \mu b}{2\sqrt{\rho}}\frac{d\rho}{d\varepsilon} \tag{1}$$

$\frac{d\rho}{d\varepsilon}$ is dependent to the operation of TWIP or TRIP/TWIP, respectively. The modelled strain-hardening rate may estimate the uniform elongation according to the Considère criterion.

Fig.4 shows the model implementation to both TWIP and TRIP/TWIP alloys. The twin volume fraction of Ti-14Mo-5Sn is lower than that of Ti-11Mo-5Sn-5Nb, causing slightly decreased plasticity. The modelled flow stress curves well agreed to the experimental data as shown in Fig.4b. The only fitting variable in the TWIP model is the twinning kinetics parameter β_{tw} which rises with reduced β stability. The strain-hardening rate is shown in Fig.4c. Although the modelled $\frac{d\sigma}{d\varepsilon}$ curves did not manage to copy the exact
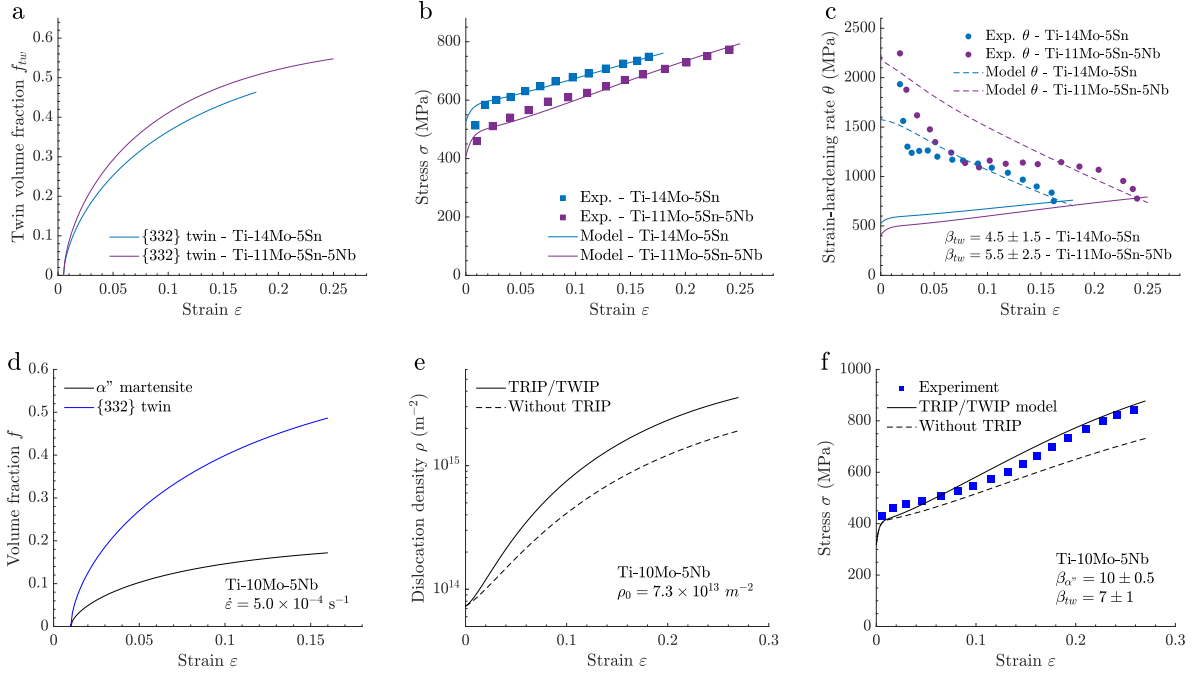
Figure 4: (a) The growing of twinning volume fraction in Ti-14Mo-5Sn and Ti-11Mo-5Sn-5Nb TWIP alloys. (b) The modelled flow stress reasonably agrees to the experimental data. (c) The experimental and modelled strain-hardening rate plots. (d) The volume fractions of both α'' martensite and $\{332\}\langle113\rangle$ twin increase with strain in Ti-10Mo-5Nb TRIP/TWIP alloy. (e) The rising of total dislocation density ρ in Ti-10Mo-5Nb. (f) Experimental and modelled stress-strain curves of Ti-10Mo-5Nb, the dashed curves display the respective evolution of dislocation density and flow stress subtracting TRIP effect.

shape of the experimental one, they captured the the point where $\frac{d\sigma}{d\varepsilon}$ dropped below the value of flow stress at the given strain rate: $\frac{d\sigma}{d\varepsilon}\big|_{\dot{\varepsilon}} = \sigma$, which effectively predicts the uniform elongation. The constitutive model integrating TRIP and TWIP was applied to Ti-10Mo-5Nb. The kinetics of $\{332\}\langle113\rangle$ twinning was more pronounced than that of $\beta \rightarrow \alpha''$ transition, making the twin fraction always higher than α'' fraction throughout the deformation (Fig.4d). The rapid increase of the transformation products significantly accelerated dislocation accumulation from the early to the intermediate deformation stage, then the rise was suppressed by dynamic recovery. Fig.4f shows the modelled mechanical behaviour reasonably agreed to the experiments. The strain-hardening rate, however, was not reproduced for the present TRIP/TWIP alloy because the hardening curve is derivative and it is more sensitive to the mechanism change, especially to the $\beta \rightarrow \alpha''$ and twinning kinetics. Virtual dislocation density (dashed curve in Fig.4e) and flow stress (dashed curve in Fig.4f) evolutions subtracting TRIP effect were predicted respectively. The flow stress still presented considerable strain-hardening solely from TWIP mode.

The goal of this work is to introduce a simple but efficient approach to implement TRIP and TWIP in Ti alloys. For this purpose, the constitutive model was ensured to use simplified but physically informed
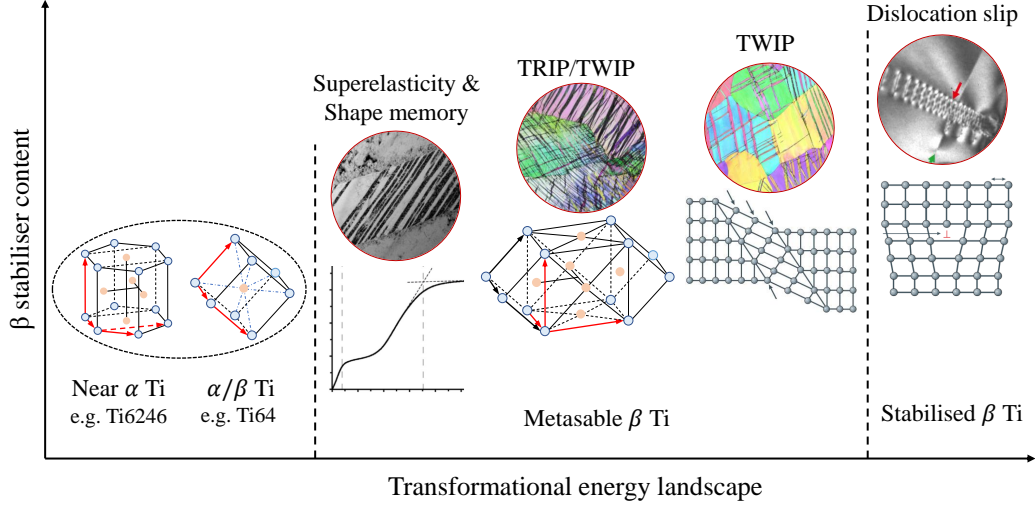
Figure 5: Transformational energy landscape and the corresponding deformation characteristics. Metastable β Ti alloys display versatile mechanical behaviours or deformation modes i.e. superelasticity [9], shape memory, TRIP/TWIP and TWIP. Dislocation slip [21] becomes the dominate deformation mode when the β is fully stabilised.

variables that govern the growing rate of twin or martensite. TWIP and TRIP may undergo jointly because of the existence of a noticeably overlapped domain in their transformational threshold energy [20], meanwhile they are mutually inclusive in terms of the transition crystallography and dislocation mechanisms. Fig.5 overviews the deformation mechanisms of Ti alloys corresponding to the transformational energy landscape. In near α and α/β alloys that present higher fraction of α' martensite, $\beta \to \alpha'$ martensitic transformation is thermally activated. By increasing the alloying elements, the high temperature β phase can be retained upon quenching and a metastable state is achievable when a pseudoelastic equilibrium is formed [22, 23]. The strain-induced martensitic transformation occurs when the transformational resistance (mainly elastic strain energy) is overcome by the joint chemical driving force and mechanical work. This group of alloys display the most versatile mechanical characteristics i.e. superelasticity, shape memory, TRIP/TWIP and TWIP. The extraordinary width of $\{332\}\langle113\rangle$ twin implies the easy nucleation and growth of $\{332\}\langle113\rangle$ twin in a layer-by-layer fashion. It effectively extends the plasticity by producing a large amount of inelastic strain within a very short time by broadening [24]. Furthermore, the spacious width entails a higher possibility to form extensive substructures such as $\{332\}\langle113\rangle_{2nd}$ or α''_{2nd} inside the wide primary twin.

In summary, we developed an efficient route to realise transformation strengthening in Ti alloys through a supervised operation of TRIP and TWIP. We carried out comprehensive study to substantiate (1) the operative deformation modes can be tailored by the underlying transition kinetics; and (2) a model with minimised internal variables can reasonably well predict the flow stress and the onset of strain localisation. A model integrating TRIP and TWIP was applied to take explicitly into account the microstructural evolution;

and the model validation quantified the noticeable contribution of $\beta \to \alpha''$ transformation to the enhanced strain-hardening. Looking forward, the modelling algorithm is extendible to broader alloy systems and the design strategy can be readily applied to industrial practice.

Acknowledgements

References

[1] T. M. Pollock, Nat. Mater. 15 (8) (2016) 809–815.

[2] K. Lu, Science 328 (5976) (2010) 319–320.

[3] J. W. Christian, Newnes, 2002.

[4] F. Sun, J. Zhang, M. Marteleur, T. Gloriant, P. Vermaut, D. Laillé, P. Castany, C. Curfs, P. Jacques, F. Prima, Acta Mater. 61 (17) (2013) 6406–6417.

[5] L. Choisez, L. Ding, M. Marteleur, H. Idrissi, T. Pardoen, P. Jacques, Nat. Comm. 11 (1) (2020) 1–8.

[6] D. Gordin, F. Sun, D. Laillé, F. Prima, T. Gloriant, How a new strain transformable titanium-based biomedical alloy can be designed for balloon expendable stents, Materialia 10 (2020) 100638.

[7] L. Lilensten, Y. Danard, C. Brozek, S. Mantri, P. Castany, T. Gloriant, P. Vermaut, F. Sun, R. Banerjee, F. Prima, Acta Mater. 162 (2019) 268–276.

[8] L. Lilensten, Y. Danard, R. Poulain, R. Guillou, J. Joubert, L. Perrière, P. Vermaut, D. Thiaudière, F. Prima, From single phase to dual-phase TRIP-TWIP alloys: design approach and properties, Materialia (2020) 100700.

[9] P. Castany, A. Ramarolahy, F. Prima, P. Laheurte, C. Curfs, T. Gloriant, Acta Mater. 88 (2015) 102–111.

[10] K. Cho, R. Morioka, S. Harjo, T. Kawasaki, H. Y. Yasuda, Scr. Mater. 177 (2020) 106–111.

[11] P. Castany, Y. Yang, E. Bertrand, T. Gloriant, Reversion of a parent $\{130\}\langle310\rangle_{\alpha''}$ martensitic twinning system at the origin of $\{332\}\langle113\rangle_{\beta}$ twins observed in metastable β titanium alloys, Phys. Rev. Lett. 117 (24) (2016) 245501.

[12] G.-H. Zhao, X. Xu, D. Dye, P. E. J. Rivera-Díaz-del-Castillo, Acta Mater. 183 (2020) 155–164.

[13] I. S. Yasnikov, A. Vinogradov, Y. Estrin, Scr. Mater. 76 (2014) 37–40.

[14] C. Brozek, F. Sun, P. Vermaut, Y. Millet, A. Lenain, D. Embury, P. Jacques, F. Prima, Scr. Mater. 114 (2016) 60–64.

[15] J. Gao, Y. Huang, D. Guan, A. J. Knowles, L. Ma, D. Dye, W. M. Rainforth, Acta Mater. 152 (2018) 301–314.

[16] X. Min, X. Chen, S. Emura, K. Tsuchiya, Scr. Mater. 69 (5) (2013) 393–396.

[17] X. Zhou, X. Min, S. Emura, K. Tsuchiya, Mater. Sci. Eng. A 684 (2017) 456–465.

[18] Y. Danard, R. Poulain, M. Garcia, R. Guillou, D. Thiaudière, S. Mantri, R. Banerjee, F. Sun, F. Prima, Materialia 8 (2019) 100507.

[19] G.-H. Zhao, X. Liang, B. Kim, P. E. J. Rivera-Díaz-del-Castillo, Mater. Sci. Eng. A 756 (2019) 156–160.

[20] G. Zhao, X. Li, N. Petrinic, npj Comput. Mater. 7 (1) (2021) 1–9.

[21] S. Kondo, T. Mitsuma, N. Shibata, Y. Ikuhara, Sci. Adv. 2 (11) (2016) e1501926.

[22] M. L. Green, M. Cohen, G. Olson, Mater. Sci. Eng. 50 (1) (1981) 109–116.

[23] G.-H. Zhao, X. Liang, X. Xu, M. Gamża, H. Mao, D. Louzguine-Luzgin, P. E. J. Rivera-Díaz-del-Castillo, Mater. Sci. Eng. A 815 (2021) 141229.

[24] S. Ogata, J. Li, S. Yip, Phys. Rev. B 71 (22) (2005) 224102.